# Precipitation Data Accuracy and Extreme Rainfall Detection for Flood Risk Analysis in the Akçay Sub-Basin

Venkataraman Lakshmi , Elif Gulen Kir * , Bin Fang

Posted Date: 20 May 2025

doi: 10.20944/preprints202505.1570.v1

Keywords: CHIRPS; Extreme Rainfall Detection; GPM-IMERG; Kolmogorov-Smirnov; Correlation of Precipitation Data; Statistical metrics

 doi:10.20944/preprints202505.1570.v1



*Article*

# Precipitation Data Accuracy and Extreme Rainfall Detection for Flood Risk Analysis in the Akçay Sub-Basin

**Venkataraman Lakshmi [1], Elif Gulen Kir [2,*] and Bin Fang [1]**

[1] Department of Civil and Environmental Engineering, University of Virginia, Charlottesville, VA 22904, USA; vl9tn@virginia.edu; bf3fh@virginia.edu

[2] Department of Civil Engineering, Faculty of Engineering and Natural Sciences, Suleyman Demirel University, Isparta, 32260, Turkey; elifgulencimen@gmail.com

* Correspondence: elifgulencimen@gmail.com

**Abstract:** This study evaluates GPM-IMERG (Global Precipitation Measurement - Integrated Multi-satellite Retrievals) and CHIRPS (Climate Hazards Group InfraRed Precipitation with Stations) satellite precipitation data in Turkey's Akçay Sub-Basin by comparing them with rain gage observations from the Finike and Elmali meteorological stations. Statistical metrics, such as Pearson's correlation coefficient, Nash-Sutcliffe Efficiency (NSE), and Root Mean Square Error (RMSE), were used to assess performance. The study also examines distributional fit via the Kolmogorov-Smirnov (K-S) test and evaluates extreme rainfall detection accuracy using metrics like Probability of Detection (POD), False Alarm Ratio (FAR), and Critical Success Index (CSI). Results indicate that GPM-IMERG agrees well with rain gage observations at the monthly scale, but less so at daily scale. The K-S test shows that the Beta distribution best fits monthly data, while the Weibull distribution better represents daily data. By comparing satellite and ground observations, this study offers insights for flood risk analysis and climate resilience strategies in regions with limited infrastructure. The evaluation of satellite precipitation in the Akçay Sub-Basin supports improved water management and strengthens regional flood monitoring. Correlating satellite and ground data enhances the utility of high-resolution satellite precipitation in data-scarce areas, enabling more accurate hydrological modeling and resilience planning.

**Keywords:** CHIRPS; extreme rainfall detection; GPM-IMERG; kolmogorov-smirnov; correlation of precipitation data; statistical metrics

## 1. Introduction

Climate change has emerged as one of the most critical challenges of the 21st century, profoundly impacting various aspects of the environment, especially precipitation patterns and water resources, with recent studies highlighting an intensification of extreme weather events and variability in hydrological cycles [1–3]. Rising global temperatures have led to significant alterations in the hydrological cycle, causing an increase in extreme weather events such as intense rainfall, floods, and droughts [4]. This intensification of precipitation not only poses risks to ecosystems and biodiversity but also endangers human lives, infrastructure, and economies [5,6]. As the frequency and severity of extreme rainfall events continue to rise, understanding and accurately assessing rainfall patterns is essential for effective water resource management, disaster prevention, and climate resilience [7–11].

In regions where meteorological stations are sparse or non-existent, specifically in remote and mountainous areas, the scarcity of ground-based rainfall data presents a major obstacle for climate-

 doi:10.20944/preprints202505.1570.v1



related studies [12]. In such areas, remotely sensed precipitation data obtained from satellite-based sources provide a valuable alternative, enabling the monitoring of rainfall across vast and inaccessible terrains [13–14]. Satellite-derived precipitation datasets, such as CHIRPS and GPM-IMERG are widely used in hydrological and agricultural research due to their high spatial and temporal resolution [15]. These datasets are invaluable for their ability to provide continuous, consistent, and global coverage, making them an essential tool for studying precipitation patterns in regions with limited ground data availability [9,16–19].

The integration and comparison of satellite rainfall data with ground-based meteorological measurements are crucial for ensuring the accuracy and reliability of remote sensing datasets [20–23]. Numerous studies have demonstrated the importance of correlating satellite-derived precipitation with in-situ data to assess the strengths and limitations of satellite observations in capturing regional rainfall characteristics [24–27]. Correlation analyses, which employ metrics such as the correlation coefficient, Nash-Sutcliffe Efficiency (NSE), and Root Mean Square Error (RMSE), help quantify the alignment between satellite data and ground observations, thereby enhancing the validity of satellite products in various applications [26,28–30]. Such evaluations not only improve the accuracy of satellite data but also strengthen their credibility for use in predictive modeling and risk assessment [18].

Moreover, statistical tests like the Kolmogorov-Smirnov (K-S) test play a valuable role in understanding the distributional characteristics of rainfall data, particularly for detecting extreme rainfall events [31]. By analyzing how well the data fits certain probability distributions (e.g., Beta, Weibull, and GEV distributions), K-S tests enable more accurate modeling of extreme events, which are vital for flood risk prediction and effective water management [32,33].

Additionally, performance metrics specific to extreme rainfall event detection, such as POD, FAR, and the CSI, provide insights into the accuracy of satellite data in identifying these events [34]. POD represents the proportion of actual extreme rainfall events correctly identified by the model, while FAR indicates the rate of incorrect alerts for extreme events [35,36]. The Critical Success Index (CSI) further combines true detections, missed events, and false alarms to give an overall performance measure of the dataset [37,38]. These metrics, along with accuracy (ACC) measures, are essential for assessing the practical reliability of satellite precipitation data for timely and effective flood risk assessment [36,39].

This study aims to compare meteorological station rain gage observations with CHIRPS and GPM-IMERG satellite datasets in Turkey's Akçay Sub-Basin, evaluating their correlation, distributional fit using the K-S test, and performance in extreme rainfall event detection through metrics like POD, FAR, and CSI. By comparing ground-based and satellite observations, this research provides insights into the potential of satellite-derived precipitation data in supporting flood risk analysis and climate resilience strategies, particularly in regions with limited meteorological infrastructure [10,19,40].

## 2. Materials and Methods

### *2.1. Study Area and Datasets*

The Akçay Sub-Basin, situated within Turkey's Western Mediterranean Basin, which is one of the country's 25 hydrological basins, covers a drainage area of 2,497 square kilometers, with elevations ranging from sea level to 3,059 meters (Figure 1). This area is characterized by extensive agricultural land use and greenhouse farming, along with a high population density. Given these characteristics, research in this region often focuses on the agricultural use of water resources. Meteorological and flow observation stations are strategically located within the Akçay Sub-Basin to capture data relevant to these studies. The locations of these observation stations are displayed in Figure 1, which provides a visual overview of the study area's spatial and environmental context.

 doi:10.20944/preprints202505.1570.v1



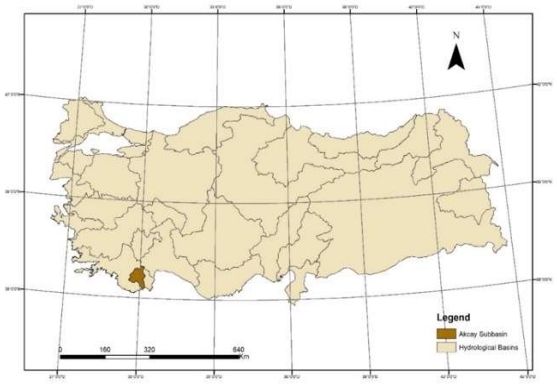


**Figure 1.** Location of the Akçay Subbasin Study Area within Turkey.

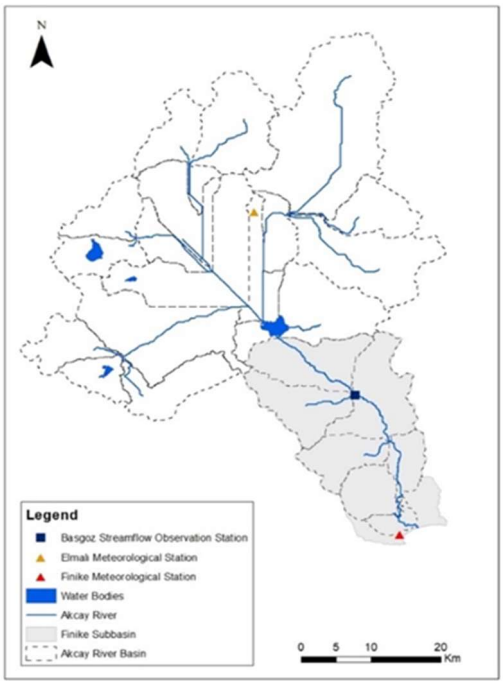


**Figure 1.** Hydrological Map of the Study Area Showing River Systems.

Watershed delineation for the Akçay Sub-Basin is carried out using the 30-meter resolution SRTM (Shuttle Radar Topography Mission) elevation data for the Western Mediterranean Basin. These digital elevation data provide a measure of the Earth's surface elevation relative to sea level, enabling the creation of a detailed elevation map [41]. After obtaining the SRTM data, they were visualized and processed within the ArcGIS program, where the data were reprojected to the appropriate geographic coordinate system. This reprojection step includes correcting resolution-based errors and filling minor gaps to improve data accuracy. Watershed delineation for the Akçay Sub-Basin is carried out using the 30-meter resolution SRTM (Shuttle Radar Topography Mission) elevation data for the Western Mediterranean Basin. These digital elevation data provide a measure of the Earth's surface elevation relative to sea level, enabling the creation of a detailed elevation map [41]. After obtaining the SRTM data, they were visualized and processed within the ArcGIS program, where the data were reprojected to the appropriate geographic coordinate system. This reprojection step includes correcting resolution-based errors and filling minor gaps to improve data accuracy.

With the elevation data refined, the river flow direction was then determined, allowing for the identification of flow accumulation areas on the map. Using these accumulation areas, watershed boundaries were established, delineating the Akçay Sub-Basin accurately. The step-by-step

 doi:10.20944/preprints202505.1570.v1



methodology used for delineating the watershed boundaries in this study area is summarized in Figure 3.

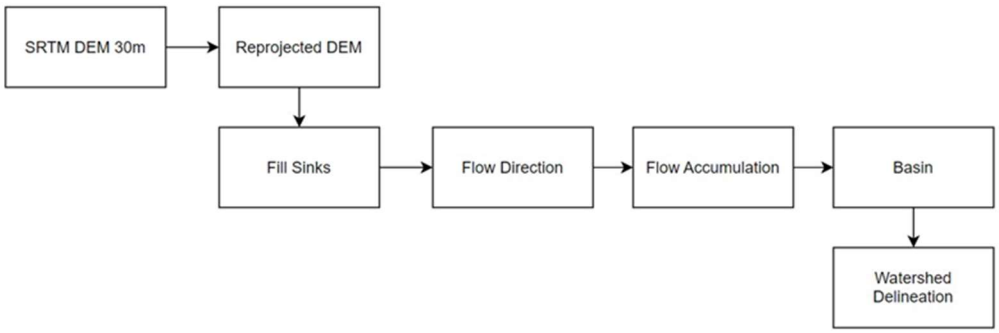


**Figure 2.** Workflow When Determining the Basin.

Figure 770. km² with an average flow rate of 3.284 m³/s from 1955-2015). Figure 3 illustrates these data: (a) a hydrograph showing the relationship between precipitation (blue bars) and stream flow (green line) from October 1, 2011, to September 30, 2015, (b) monthly precipitation at Finike Station, revealing seasonal rainfall patterns with winter peaks and summer declines, and (c) monthly precipitation at Elmali Station, highlighting variability within the Akçay Sub-Basin. Peaks in rainfall during 2012 and 2015 correspond to high flow rates, underscoring the basin's sensitivity to intense precipitation events. These data provide critical insights for water resource management in this region.

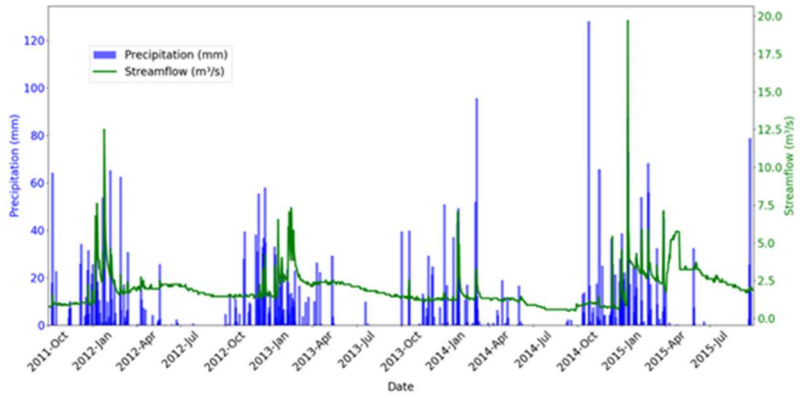


(a)

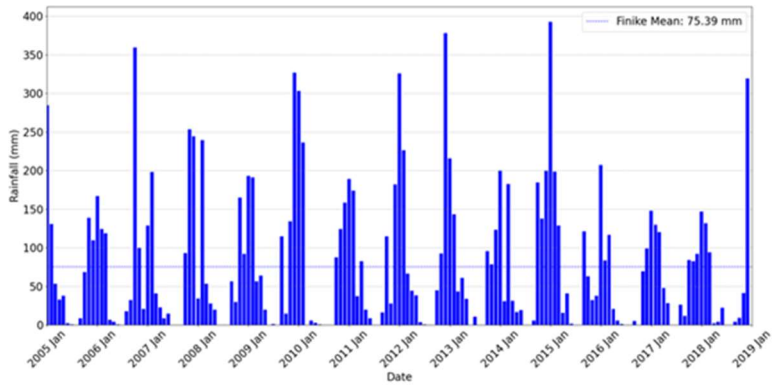


(b)

 doi:10.20944/preprints202505.1570.v1



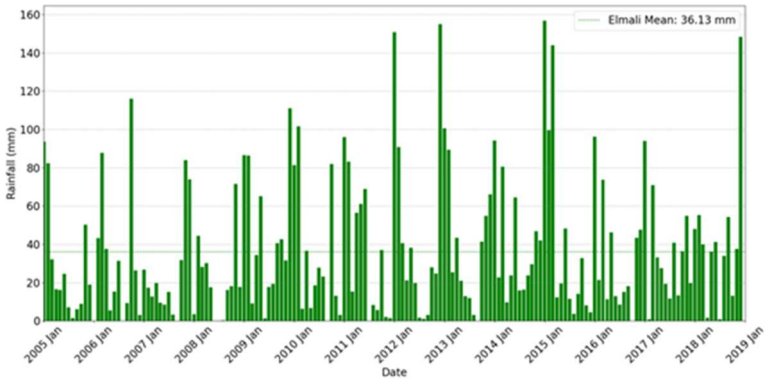


**(c).**

**Figure 3.** (a) Daily Hydrograph of Finike Sub-Basin (October 1, 2011 - September 30, 2015), (b) Monthly precipitation at the Finike Station, (c) Monthly precipitation at the Elmali Station (2005-2018).

The data presented in Figure 3a illustrate a direct relationship between precipitation and flow rates at the Basgoz Catallar station. High-precipitation events, particularly in January 2015, December 2014, and January 2013, resulted in notable increases in flow rates. For instance, on January 13, 2015, 87.3 mm of precipitation led to a peak flow rate of 19.7 $m^3/s$. Similarly, 49.2 mm of rain on January 27, 2014, produced a flow rate of 4.4 $m^3/s$, and 18.2 mm of precipitation on February 8, 2013, generated 6.07 $m^3/s$. Following the peak flows triggered by intense rainfall events, the streamflow rates typically showed a significant decline within a few days. For instance, after the peak of 19.7 $m^3/s$ on January 13, 2015, the flow rate dropped to approximately 6.13 $m^3/s$ by January 14, 2015, representing a reduction of about 68% in one day as the precipitation intensity decreased. Similarly, in other instances, streamflow reduced by roughly 50-70% within one or two days following high-precipitation events. This pattern highlights the basin's hydrological response to intense rainfall events, underscoring the role of precipitation monitoring in water resource management.

Figure 3b displays the monthly precipitation at the Finike Meteorological Observation Station from 2005 to 2018, revealing a clear seasonal pattern with peaks in winter and declines in summer. Notably, extreme rainfall events, such as those in January 2015 (392.6 mm, compared to the long-term average of 75.39 mm) and December 2012 (378.2 mm), indicate periods of high-water availability, which are critical for developing effective water management strategies.

Figure 3c shows the monthly precipitation data for the Elmali Meteorological Station over the same period, highlighting variability within the Akçay Sub-Basin. The average monthly precipitation is 36.13 mm, with winter and spring showing higher levels. Rainfall events above 100 mm, as recorded in January 2015 (156.8 mm) and December 2012 (155.0 mm), compared to the average value at 36.13 mm, emphasize the importance of localized data for water resource management and agricultural planning.

Precipitation data can be acquired through ground-based rain gauge stations and satellite sensors. While rain gauges provide reliable data, their spatial and temporal limitations, especially in complex terrains, can hinder comprehensive precipitation analysis. To address these limitations, this study utilized high-resolution remote sensing data from CHIRPS and GPM-IMERG, known for their extensive spatial and temporal coverage. CHIRPS, with a 0.05° spatial resolution, combines ground and satellite observations, offering consistent precipitation data from 1981 to the present, suitable for hydrological and agricultural applications [15]. GPM-IMERG, available since 2000, provides global precipitation data at 0.1° resolution, making it valuable for short-term and extreme event analysis [14].

Both CHIRPS (Version 2.0) and GPM-IMERG (Final Run, V06) precipitation datasets were processed in Python (Jupyter Notebook) and tailored to the study area. CHIRPS data were obtained from the Climate Hazards Center (https://www.chc.ucsb.edu/data/chirps) and GPM-IMERG data from NASA's Precipitation Processing System portal (https://gpm.nasa.gov/data/imerg) The datasets

 doi:10.20944/preprints202505.1570.v1



were reprocessed to improve spatial resolution and adjust temporal intervals to better fit the requirements of the regional analysis. This pre-processing enabled a more accurate correlation analysis with ground-based observations. Table 1 summarizes the main characteristics of these remotely sensed precipitation datasets.

**Table 1.** Characteristics of Remotely Sensed Datasets Used in the Analysis.

| Remotely Data Sets (Precipitation) | Temporal Coverage | Temporal Resolution | Spatial Resolution | File Format |
|---|---|---|---|---|
| CHIRPS (Observation) | 1981-Present | Daily | 0.05° | netCDF |
| GPM-IMERG (Observation) | 2000- Present | Daily, half hourly | 0.1° | netCDF |

In this study, CHIRPS and GPM-IMERG datasets were utilized to analyze rainfall patterns in Turkey's Akçay Sub-Basin, and these datasets were compared with ground-based meteorological data. While satellite-derived datasets have been validated in previous studies for hydrological and climate analyses [18,42,43], localized assessments are often lacking. This research addresses the unique topographical and climatic features of the Akçay Sub-Basin, where rainfall patterns are highly variable due to complex terrain and frequent extreme events.

The accuracy of CHIRPS and GPM-IMERG data was evaluated at both monthly and daily timescales, providing a fine-scale analysis critical for flood-prone regions. Beyond general accuracy metrics, the dataset performance in detecting extreme rainfall events was assessed using specialized metrics—POD, FAR and CSI—to gauge their reliability for real-time monitoring and disaster preparedness in areas with sparse observational networks.

Overall, this study contributes a comprehensive evaluation of satellite precipitation data specifically tailored to the Akçay Sub-Basin, offering valuable insights that can enhance water management strategies and support local flood monitoring efforts in Turkey's complex terrain.

### *2.2. Correlation Analysis Between Meteorological Station and Remotely Sensed Data Sets*

Comparing rainfall data from meteorological stations with remotely sensed precipitation data is essential for validating satellite-derived datasets. This study employs various analytical methods to evaluate the alignment between ground-based and satellite precipitation data, including the correlation coefficient (r) [44], Nash-Sutcliffe Efficiency (NSE) [28], Root Mean Square Error (RMSE) [45], Percent Bias (PBIAS) [29], and Mean Absolute Error (MAE) [46]. These metrics are vital for assessing the degree of correlation between the ground-based observations and remotely sensed data, thereby evaluating the reliability of satellite-derived measurements.

Each of these metrics provides unique insights into the relationship between the datasets: the correlation coefficient (r) measures the linear relationship between two datasets; NSE evaluates the alignment between model predictions and observations; RMSE quantifies the average deviation of predictions from actual observations; PBIAS indicates the average bias in the model's predictions compared to observations; and MAE assesses the absolute and percentage magnitude of prediction errors, respectively [18,47–49].

In the equations, $O_i$ represents the observed values, $P_i$ the model or predicted values, $\bar{O}$ the mean of the observed values, $\bar{P}$ the mean of the predicted values, and n denotes the number of observations.

$$r = \frac{\sum_{i=1}^{n}(O_i - \bar{O})(P_i - \bar{P})}{\sqrt{\sum_{i=1}^{n}(O_i - \bar{O})^2 \sum_{i=1}^{n}\left(P_j - \bar{P}\right)^2}} \quad (1)$$

$$NSE = \frac{\sum_{i=1}^{n}(O_i - P_i)^2}{\sum_{i=1}^{n}(O_i - \bar{O})^2} \quad (2)$$

 doi:10.20944/preprints202505.1570.v1



$$RMSE = \sqrt{\frac{1}{n}\sum_{i=1}^{n}(P_i - O_i)^2} \quad (3)$$

$$PBIAS = 100 \times \frac{\sum_{i=1}^{n}(P_i - O_i)}{\sum_{i=1}^{n} O_i} \quad (4)$$

$$MAE = \frac{1}{n}\sum_{i=1}^{n}|P_i - O_i| \quad (5)$$

For this study, correlation analyses were conducted on precipitation data from the Finike and Elmali meteorological stations in conjunction with the CHIRPS and GPM-IMERG remote sensing datasets, covering the period from 2005 to 2018. These analyses provide insights into the extent to which satellite-derived data correlate with meteorological station observations and the accuracy of the precipitation estimates. Table 2 presents the monthly correlation analysis results, comparing data from the Finike and Elmali stations with the CHIRPS and GPM-IMERG datasets.

**Table 2.** Monthly Analysis Results (January 1, 2005, and December 31, 2018).

| Statistical Metrics | Elmali | | Finike | |
|---|---|---|---|---|
| | CHIRPS | GPM-IMERG | CHIRPS | GPM-IMERG |
| Correlation Coefficient (r) | 0.765 | 0.818 | 0.899 | 0.943 |
| Nash-Sutcliffe Efficiency (NSE) | -0.993 | -0.549 | 0.679 | 0.887 |
| Root Mean Square Error (RMSE) (mm) | 49.682 | 43.800 | 50.813 | 30.146 |
| Percent Bias (PBIAS) (%) | 71.698 | 65.283 | 19.045 | -4.870 |
| Mean Absolute Error (MAE) (mm) | 32.133 | 28.056 | 30.811 | 18.117 |

According to Table 2, the GPM-IMERG dataset exhibits higher correlation coefficients than CHIRPS for both Elmali and Finike stations (Elmali: 0.818, Finike: 0.943), indicating a stronger linear relationship between GPM-IMERG data and ground-based meteorological observations. The GPM-IMERG dataset performed best at the Finike station, with a high and positive Nash-Sutcliffe Efficiency (NSE) value of 0.887, which suggests a strong linear agreement with observed data. In contrast, both datasets for the Elmali station displayed negative NSE values, indicating greater deviations from observed data; however, the NSE for GPM-IMERG (-0.549) was still better than that for CHIRPS (-0.993).

The Root Mean Square Error (RMSE) values for GPM-IMERG were also lower than those for CHIRPS at both stations (Elmali: 43.800 mm vs. 49.682 mm; Finike: 30.146 mm vs. 50.813 mm), reflecting less error in GPM's precipitation predictions. Furthermore, the Percent Bias (PBIAS) for GPM-IMERG at the Elmali station (65.283 %) was lower than that of CHIRPS, while the negative bias at the Finike station (-4.870 %) suggests minimal systematic deviation from observations, highlighting the accuracy of GPM-IMERG data in this region. Additionally, GPM-IMERG data showed lower Mean Absolute Error (MAE) values (Elmali: 28.056 mm, Finike: 18.117 mm).

Overall, the GPM-IMERG dataset for Finike exhibited the best performance across all statistical metrics, achieving the closest alignment with observed data. In contrast, CHIRPS data showed notably lower performance at the Elmali station, with higher error rates and greater deviations from observed values.

Table 3 summarizes the results of the daily correlation analysis for the Finike and Elmali meteorological stations, comparing the CHIRPS and GPM-IMERG remote sensing datasets.

 doi:10.20944/preprints202505.1570.v1



**Table 3.** Daily Analysis Results (January 1, 2005, and December 31, 2018).

| Statistical Metrics | Elmali | | Finike | |
|---|---|---|---|---|
| | CHIRPS | GPM-IMERG | CHIRPS | GPM-IMERG |
| Correlation Coefficient (r) | 0.345 | 0.420 | 0.350 | 0.592 |
| Nash-Sutcliffe Efficiency (NSE) | -2 | -0.868 | -0.697 | 0.239 |
| Root Mean Square Error (RMSE) (mm) | 7.367 | 5.812 | 12.455 | 8.341 |
| Percent Bias (PBIAS) (%) | 71.466 | 65.060 | 19.291 | -4.673 |
| Mean Absolute Error (MAE) (mm) | 2.384 | 2.034 | 3.772 | 2.632 |

As shown in Table 3, the daily analysis results reveal that GPM-IMERG data also exhibit higher correlation coefficients than CHIRPS data for both Elmali (0.420) and Finike (0.592) stations, indicating a stronger linear relationship with meteorological station data. The GPM-IMERG data for the Finike station again showed the best performance with a positive NSE value (0.239), whereas the NSE values for Elmali were negative for both datasets, suggesting deviations from observed data. Nevertheless, the NSE for GPM-IMERG in Elmali (-0.868) was an improvement over that of CHIRPS (-2.000).

In terms of RMSE, GPM-IMERG data also demonstrated lower values at both stations (Elmali: 5.812 mm, Finike: 8.341 mm), indicating a reduced error in daily precipitation predictions. The bias values for GPM-IMERG were lower compared to CHIRPS, with the negative PBIAS at the Finike station (-4.673 %) suggesting minimal systematic deviation, which enhances the accuracy of GPM-IMERG data. Furthermore, GPM-IMERG data showed lower MAE values at both stations (Elmali: 2.034 mm, Finike: 2.632 mm), reflecting smaller average errors.

To further examine the relationship between GPM-IMERG precipitation data and the Finike meteorological station data, detailed analyses were conducted on both monthly and daily scales. This involved calculating Pearson's correlation coefficient [44] and Spearman's Rho [50], along with performing linear regression analysis [51]. The Pearson correlation coefficient $r$ is defined as follows, where $x_i$ and $y_i$ are observations of the $x$ and $y$ variables, respectively, and $\bar{x}$ and $\bar{y}$ are the means of the $x$ and $y$ variables. The Spearman correlation coefficient $\rho$ is defined as follows, where $d_i$ represents the rank differences between $x_i$ and $y_i$ observations, and $n$ is the number of observations.

$$r = \frac{\sum(x_i - \bar{x})(y_i - \bar{y})}{\sqrt{\sum(x_i - \bar{x})^2}\sqrt{\sum(y_i - \bar{y})^2}} \tag{6}$$

$$\rho = 1 - \frac{6\Sigma\, d_i^2}{n(n^2 - 1)} \tag{7}$$

Linear regression analysis is a statistical method that examines the relationship between two or more variables and aims to determine how a dependent variable is affected by one or more independent variables. In this context, $y$ represents the dependent variable, $x$ represents the independent variable, $\beta_0$ represents the independent variable, $\beta_1$ is the slope coefficient, and $\epsilon$ is the error term.

$$\beta_1 = \frac{\sum(x_i - \bar{x})(y_i - \bar{y})}{\sum(x_i - \bar{x})^2} \tag{8}$$

$$\beta_0 = \bar{y} - \beta_1\bar{x} \tag{9}$$

For monthly rainfall data, the Pearson correlation coefficient was 0.943 and Spearman's Rho was 0.951, both indicating a very strong positive correlation between GPM-IMERG data and ground observations at the Finike station. Linear regression analysis yielded a slope of 0.871, an intercept of

 doi:10.20944/preprints202505.1570.v1



6.046, a standard error of 0.024, and an R-squared value of 0.889, suggesting a robust alignment between satellite-derived and observed precipitation data, as shown in Figure 4a.

For daily rainfall data, the Pearson correlation coefficient was 0.592, and Spearman's Rho was 0.499, indicating a moderate positive correlation. Linear regression analysis resulted in a slope of 0.547, an intercept of 1.005, a standard error of 0.010, and an R-squared value of 0.35. Although the correlation at the daily scale was lower compared to monthly data, it still demonstrates a statistically significant relationship, as shown in Figure 4b.

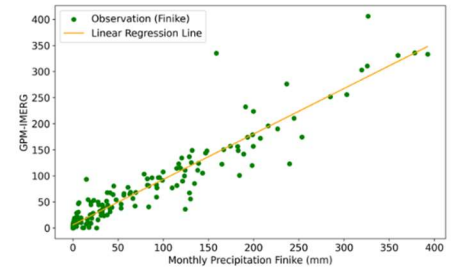


(a)

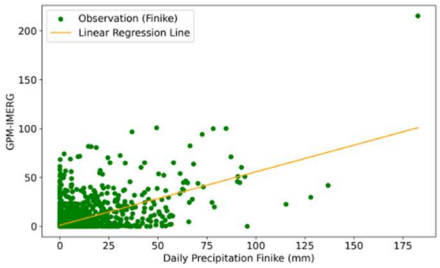


(b)

**Figure 4.** (a) Monthly Precipitation Comparison between Finike Meteorological Station and GPM-IMERG Data, (b) Daily Precipitation Comparison between Finike Meteorological Station and GPM-IMERG Data.

As shown in Figure 4, linear regression analysis between observed precipitation at the Finike meteorological station and satellite-based GPM-IMERG data reveals that GPM-IMERG explains 88.9% of the variance in observed monthly precipitation, while capturing only 35% of the variability in daily data. This indicates that GPM-IMERG is a reliable source for capturing monthly rainfall patterns. The strong alignment between satellite data and ground observations at the monthly scale suggests that satellite data accuracy improves over larger time scales. However, the lower performance at the daily scale highlights the challenges satellite products face in detecting short-duration precipitation events. Previous studies have shown that GPM-IMERG may either underestimate or overestimate precipitation extremes, particularly in arid or mountainous regions and during flash flood conditions [47,52–54].

Therefore, satellite-based precipitation data are particularly reliable at the monthly scale but may struggle to fully capture the variability of daily rainfall events. Consequently, while GPM-IMERG data are suitable for monthly analyses, daily analyses require cautious interpretation due to higher variability. To gain a more detailed understanding of rainfall event distribution characteristics, further analyses, such as the Kolmogorov-Smirnov (K-S) test, are recommended.

## 3. Results

### *3.1. Kolmogorov-Smirnov (K-S) Tests and Probability Distribution Analysis*

In this section, Kolmogorov-Smirnov (K-S) tests [31] and probability distribution analyses were conducted to examine the distributional characteristics of the rainfall data obtained from the Finike meteorological station. These tests were used to evaluate how well the rainfall data fit specific

 doi:10.20944/preprints202505.1570.v1



probability distributions, allowing for a more accurate modeling of extreme rainfall events. The study investigated various distributions, including Gamma [55], Lognormal [56], Normal [57], Weibull [58], Exponential [59], Gumbel [60], Pareto [61], Beta [59], and Generalized Extreme Value (GEV) [62]. The K-S test results for both monthly and daily rainfall data are summarized in Table 4, with distributions showing smaller K-S statistic values and larger p-values indicating a better fit to the data.

**Table 4.** Kolmogorov-Smirnov (K-S) Test Results.

| Distributions | Monthly Dataset | | Daily Dataset | |
|---|---|---|---|---|
| | Statistic | p-value | Statistic | p-value |
| Gamma | 0.12 | 0.013 | 0.42 | 0.001 |
| Lognormal | 0.17 | 0.001 | 0.41 | 0.001 |
| Normal | 0.75 | 0.001 | 0.54 | 0.001 |
| Weibull | 0.14 | 0.003 | 0.36 | 0.001 |
| Exponential | 0.22 | 0.001 | 0.75 | 0.001 |
| Gumbel | 0.15 | 0.001 | 0.47 | 0.001 |
| Pareto | 0.30 | 0.001 | 0.70 | 0.001 |
| Beta | 0.11 | 0.033 | 0.43 | 0.001 |
| Generalized Extreme Value | 0.36 | 0.001 | 0.58 | 0.001 |

Based on the K-S test results, the most suitable probability distributions for the monthly and daily rainfall datasets at the Finike meteorological station were identified. For the monthly dataset, the Beta distribution demonstrated the best fit (K-S statistic = 0.11, p-value = 0.033), while the Weibull distribution provided the best fit for the daily dataset (K-S statistic = 0.36, p-value = 0.001), indicating that daily rainfall data align well with this distribution.

Figure 5a shows a histogram and Probability Density Function (PDF) for the monthly rainfall data fitted to the Beta distribution, highlighting a strong alignment for lower rainfall values. Figure 5b displays the Cumulative Distribution Function (CDF) of the normalized monthly rainfall data with respect to the Beta distribution.

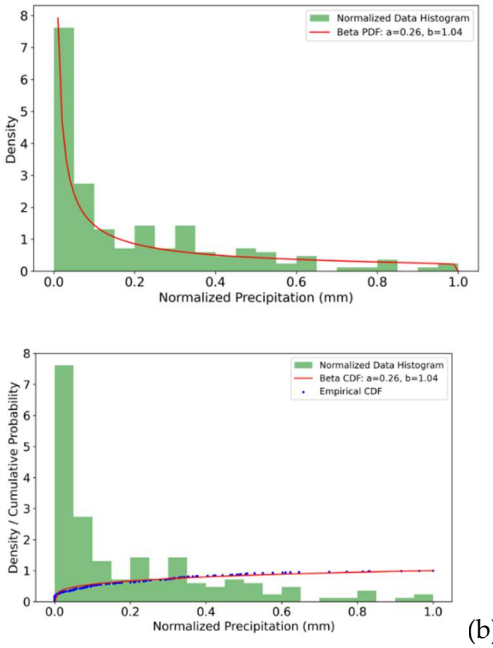


**Figure 5. (a)** Histogram and PDF Plot for Finike Monthly Precipitation Data with Beta Distribution, (b) CDF Plot for Normalized Monthly Precipitation Data.

Figures 5a and 5b reveal that lower rainfall values (in the range of 0.0-0.2 mm) are predominant, with the Beta distribution (red curve) accurately reflecting this trend. Although the fit declines for

 doi:10.20944/preprints202505.1570.v1



higher rainfall values, the overall distribution is well-represented by the Beta distribution, especially in the case of low rainfall events. In Figure 5a, the Probability Density Function (PDF) illustrates how the Beta distribution aligns closely with the histogram (green bars) of observed rainfall values, capturing the high frequency of lower values effectively. Figure 5b, showing the Cumulative Distribution Function (CDF), further supports this by depicting a steep increase in cumulative probability at lower rainfall values, confirming that a large portion of the data lies in this range. The empirical CDF (blue dots) shows the cumulative probability of the normalized data, representing the proportion of values less than or equal to a given point. This alignment suggests that the Beta distribution is a suitable model for the dataset, especially when analyzing the likelihood of low rainfall occurrences. Figures 6a and 6b illustrate the Probability Density Functions (PDFs) and threshold values for monthly and daily rainfall data, respectively, highlighting the identification of extreme rainfall events.

Figures 6a and 6b illustrate the Probability Density Functions (PDFs) and threshold values for monthly and daily rainfall data, respectively, highlighting the identification of extreme rainfall events.

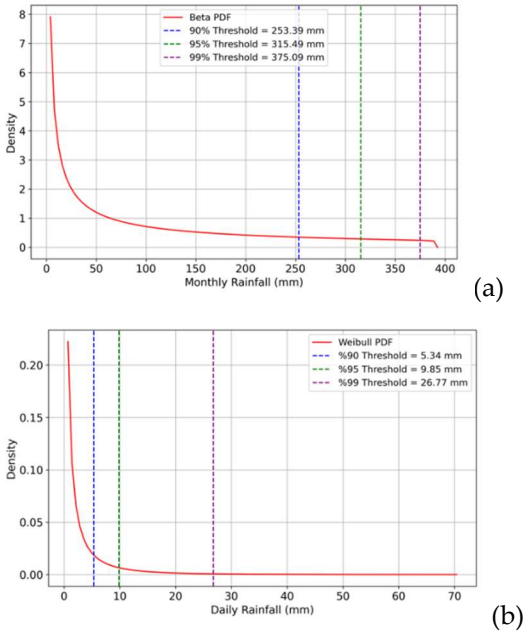


**Figure 6.** (a) Beta Distribution with Threshold Values for Monthly Rainfall Data, (b) Weibull Distribution with Threshold Values for Daily Rainfall Data.

Figure 6a presents the threshold analysis for monthly rainfall data. The 90%, 95%, and 99% threshold lines are positioned at approximately 253.39 mm, 315.49 mm, and 375.09 mm, respectively. In the dataset, 9 rainfall events exceeded the 90th percentile threshold, marking periods of significant hydrological risk due to potential flood and waterlogging (e.g., 284.8 mm, 359.6 mm, 253.4 mm). These thresholds delineate boundaries for extreme monthly rainfall, enabling the identification of high-risk months. Monthly rainfall exceeding the 99th percentile (375.09 mm) signifies exceptionally high rainfall, indicating some of the most intense and disruptive hydrological events of the year.

Figure 6b shows the daily rainfall data fitted to a Weibull distribution, with thresholds of 5.34 mm for the 90th percentile, 9.85 mm for the 95th percentile, and 26.77 mm for the 99th percentile. In this dataset, 23 rainfall events surpassed the 90th percentile, while only 8 events exceeded the 99th percentile (e.g., 53.0 mm, 46.4 mm, and 70.4 mm), identifying rare, high-risk events. These thresholds are critical for identifying days with heightened hydrological risk, where even a single extreme rainfall event may lead to infrastructure strain and rapid-onset flooding. These threshold analyses provide a foundation for evaluating how effectively extreme rainfall events can be detected using satellite and ground data.

 doi:10.20944/preprints202505.1570.v1



*3.2. Performance of Extreme Rainfall Event Detection*

To evaluate the accuracy of extreme rainfall event detection from the Finike meteorological station and GPM-IMERG satellite data, several performance metrics were used, including POD, FAR, POFD, CSI, and ACC [34,63,64]. These metrics provide insights into detection success and error rates, with POD indicating correctly detected extreme events, FAR representing false positive rates, POFD showing misclassified non-extreme events, CSI evaluating overall detection success while accounting for errors, and ACC representing total detection accuracy. The formulas used are:

$$POD = \frac{TP}{TP + FN} \quad (10)$$

$$FAR = \frac{FP}{TP + FP} \quad (11)$$

$$POFD = \frac{FP}{FP + TN} \quad (12)$$

$$CSI = \frac{TP}{TP + FP + FN} \quad (13)$$

$$ACC = \frac{TP + TN}{TP + TN + FP + FN} \quad (14)$$

where TP (True Positive) represents correctly detected extreme rainfall events, FN (False Negative) denotes extreme events that were not identified, FP (False Positive) refers to non-extreme events that were incorrectly classified as extreme, and TN (True Negative) corresponds to correctly identified non-extreme events.

The threshold values determined from Finike meteorological station rainfall data—253.39 mm for the 90th percentile of monthly rainfall and 5.34 mm for the 90th percentile of daily rainfall—served as input parameters for calculating performance metrics to evaluate the accuracy of satellite-based extreme rainfall detection. Rainfall events exceeding these thresholds were classified as "extreme rainfall," providing a critical reference point for assessing the GPM-IMERG satellite data's capability in identifying extreme events. By employing these threshold values, the satellite data's ability to accurately detect extreme rainfall events was assessed, and the performance metrics are presented in Table 5.

**Table 5.** Performance Comparison for Monthly and Daily Rainfall Data from Finike Meteorological Station and GPM-IMERG.

| Performance Metrics | Monthly Comparison (Finike vs. GPM-IMERG) | Daily Comparison (Finike vs. GPM-IMERG) |
|---|---|---|
| POD (Probability of Detection) | 0.778 | 0.478 |
| FAR (False Alarm Ratio) | 0.222 | 0.388 |
| POFD (Probability of False Detection) | 0.013 | 0.048 |
| CSI (Critical Success Index) | 0.636 | 0.366 |
| ACC (Accuracy) | 0.976 | 0.887 |

According to Table 5, the GPM-IMERG dataset shows strong performance in detecting extreme rainfall events for monthly data. Using a 253.9 mm threshold, the dataset achieved a high detection rate (POD: 0.778) and low false alarm rate (FAR: 0.222), with a minimal Probability of False Detection (1.3%) and high accuracy (ACC: 97.6%). These values suggest that GPM-IMERG data are effective for monthly extreme event identification.

In contrast, when applied to daily rainfall data with a threshold of 5.34 mm, the detection rate was lower (POD: 0.478), and the false alarm rate was higher (FAR: 0.388), with an overall accuracy of 88.7% (ACC: 0.887). These findings indicate that, while GPM-IMERG data perform reliably for

 doi:10.20944/preprints202505.1570.v1



monthly extreme event detection, the accuracy in identifying daily extremes could benefit from further enhancement, likely due to the increased temporal variability at finer scales.

## 4. Conclusions

This study assessed the accuracy and effectiveness of GPM-IMERG and CHIRPS satellite precipitation data in comparison with ground-based observations from the Finike and Elmali meteorological stations, focusing on extreme rainfall events in Turkey's Finike Sub-Basin. The analysis encompassed monthly and daily precipitation data, employing various statistical and performance metrics to evaluate the correlation, error rates, and suitability of GPM-IMERG data for hydrological applications.

Results showed that GPM-IMERG data aligned more closely with ground observations than CHIRPS data, particularly for monthly data, with Pearson and Spearman correlation coefficients of 0.943 and 0.951, respectively, and lower error metrics (RMSE: 50.813 mm, MAE: 30.811 mm). In contrast, daily correlation was weaker, with Pearson and Spearman coefficients of 0.592 and 0.499, and higher error metrics (RMSE: 12.455 mm, MAE: 3.772 mm). This suggests that GPM-IMERG data are more effective for capturing long-term precipitation trends than short-term daily variations. The improved agreement at the monthly scale may result from the averaging of overestimations and underestimations over time, leading to a reduction in overall bias. However, at the daily scale, discrepancies between satellite estimates and ground observations remain more pronounced, likely due to the higher variability and localized nature of precipitation events.

The Kolmogorov-Smirnov (K-S) tests identified the Beta distribution as the best fit for monthly rainfall data (K-S statistic = 0.11, p-value = 0.033) and the Weibull distribution for daily data (K-S statistic = 0.36, p-value = 0.001), providing a basis for more accurate flood risk assessments and water management strategies. The 90th percentile threshold values, set at 253.39 mm for monthly data and 5.34 mm for daily data, played a critical role in defining extreme rainfall events and served as a consistent benchmark for evaluating the GPM-IMERG dataset's detection capabilities. Extreme rainfall detection performance indicated that GPM-IMERG data reliably identified monthly extreme events, achieving a high Probability of Detection (POD: 0.778), low False Alarm Ratio (FAR: 0.222), and high overall accuracy (ACC: 97.6%). For daily data, the detection rate was lower (POD: 0.478), with a higher false alarm rate (FAR: 0.388) and overall accuracy of 88.7%, highlighting the need for improved precision in daily rainfall estimates.

In conclusion, GPM-IMERG data are suitable for monitoring monthly precipitation and identifying extreme rainfall events on a broader temporal scale. The dataset proves valuable for regional hydrological applications and flood risk assessment, particularly in areas lacking dense meteorological station networks. Nonetheless, for applications requiring finer temporal precision, such as daily flood forecasting, supplementary ground-based observations or enhanced satellite methods may be necessary. Future studies could focus on refining satellite data for daily event detection and exploring hybrid approaches that integrate both satellite and in-situ data for enhanced accuracy in short-term precipitation analysis. In future modeling and research, leveraging the correlation between satellite data and meteorological station observations could significantly enhance the utility of high temporal resolution satellite-derived precipitation data, especially in regions lacking detailed ground-based observations, thereby supporting more accurate hydrological applications and climate resilience strategies.

## 5. Discussion and Future Work

This study evaluates the reliability and accuracy of GPM-IMERG and CHIRPS satellite-based precipitation data in the Akçay Sub-Basin, located within the Western Mediterranean Basin of Turkey. The correlation between satellite-based precipitation data and ground observations from Finike and Elmali meteorological stations was analyzed. To detect extreme precipitation events, distribution fit analyses were conducted, and the accuracy of satellite data in capturing extreme

 doi:10.20944/preprints202505.1570.v1



precipitation was assessed using various performance metrics. The findings of the study provide crucial information that contributes to the development of resilience strategies against climate change specific to the Akçay Sub-Basin.

The results obtained in the Akçay Sub-Basin are consistent with studies suggesting that satellite-based precipitation data can be beneficial for hydrological applications in areas with limited ground data. In this context, studies conducted within Turkey by [65] highlight that CHIRPS data is reliable in semi-arid regions but limited in accuracy over mountainous areas. [66,67] evaluated the performance of grid-based and satellite-based precipitation data in Turkey, emphasizing the role of satellite data in water resource management. [68,69] and [70,71] explored the potential of IMERG data for identifying extreme rainfall and flood events.

Internationally, [10] emphasized the usefulness of satellite precipitation estimates in monitoring hydro-meteorological events. [11] compared the accuracy of CHIRPS and TRMM Multi-satellite Precipitation Analysis (TMPA) data in the Mekong River Basin, demonstrating the reliability of CHIRPS data. [18] evaluated the adequacy of CHIRPS and GPM IMERG data for hydraulic modeling in Vietnam basins, supporting their usability in hydrometeorological analyses. Additionally, [26] assessed the reliability of high-resolution TMPA data within the U.S., and [47] examined the performance of satellite-based products such as GPM IMERG and TRMM over the past two decades. These studies align with the findings of our analysis in the Akçay Sub-Basin, supporting the reliability of CHIRPS and GPM IMERG data, especially in complex topographic areas and at monthly scales.

This study demonstrates that GPM-IMERG data captures extreme precipitation events with greater accuracy than CHIRPS in the Akçay Sub-Basin. The comparison of data accuracy at daily and monthly scales also reveals the limitations of satellite data in applications requiring high temporal resolution. This finding underscores the necessity of practical recommendations for integrating satellite data with ground observations, especially in topographically complex regions.

The findings of this study can be extended to other basins within Turkey. Regions with diverse climatic and topographic characteristics, such as the high rainfall areas of the Black Sea and the semi-arid basins of Central Anatolia, present potential areas where these analyses can be applied. Specifically, it is essential to examine the accuracy of satellite data in capturing intense rainfall events, particularly in the steep terrains and high-rainfall areas of the Eastern Black Sea. Future studies should consider the use of advanced algorithms and hybrid models to improve the accuracy of satellite-based precipitation data at daily scales. Hybrid models could enable more precise short-term forecasts with high-resolution data. Additionally, artificial intelligence and machine learning approaches that combine satellite data with ground observations may enhance the detection of extreme precipitation events.

In conclusion, this study in the Akçay Sub-Basin demonstrates that satellite-based precipitation data is a reliable monitoring tool at monthly scale. The study observed that GPM-IMERG data captures extreme events with higher accuracy than CHIRPS. The widespread application of such studies across Turkey would contribute to sustainable water resource management and disaster risk reduction strategies, supporting more effective planning.

**Author Contributions:** Conceptualization, V.L., E.G.K., and B.F.; methodology, E.G.K. and B.F.; software, E.G.K.; validation, V.L. and B.F.; formal analysis, E.G.K.; investigation, E.G.K.; resources, V.L.; data curation, E.G.K.; writing—original draft preparation, E.G.K.; writing—review and editing, V.L. and B.F.; visualization, E.G.K.; supervision, V.L. All authors have read and agreed to the published version of the manuscript.

**Funding:** The APC was fully waived for this article thanks to an invitation extended to Prof. Dr. Venkataraman Lakshmi by the journal. No other external funding was received for this research.

**Acknowledgments:** The author Elif Gulen Kir thanks the Turkish State Meteorological Service (MGM) for providing meteorological data, and the Scientific and Technological Research Council of Türkiye (TÜBİTAK) for their financial and technical support (grant number 1059B142201431). The author Elif Gulen Kir also thanks Prof. Dr. Venkataraman Lakshmi's team and institution for their academic collaboration and support throughout this

 doi:10.20944/preprints202505.1570.v1



research. The authors have reviewed and edited the output and take full responsibility for the content of this publication.

**Conflicts of Interest:** The authors declare no conflicts of interest. The funders had no role in the design of the study; in the collection, analyses, or interpretation of data; in the writing of the manuscript; or in the decision to publish the results.

## References


1. Intergovernmental Panel on Climate Change. Climate Change 2021: The Physical Science Basis; Cambridge University Press: Cambridge, UK, 2021. https://doi.org/10.1017/9781009157896.
2. Ali, S.; Zhang, Q.; He, Y. Impacts of climate change on extreme precipitation and river flow in Asia: A systematic review. J. Hydrol. 2022, 602, 126689. https://doi.org/10.1016/j.jhydrol.2021.126689.
3. Gudmundsson, L.; Decharme, B.; Blöschl, G. Observed climate variability and extremes in global river flow. Nat. Rev. Earth Environ. 2023, 4, 44–59. https://doi.org/10.1038/s43017-022-00303-6.
4. Westra, S.; Fowler, H.J.; Evans, J.P.; Alexander, L.V.; Berg, P.; Johnson, F.; Kendon, E.J.; Lenderink, G.; Roberts, N.M. Future changes to the intensity and frequency of short-duration extreme rainfall. Rev. Geophys. 2014, 52, 522–555. https://doi.org/10.1002/2014RG000464.
5. Dottori, F.; Szewczyk, W.; Ciscar, J.-C.; Zhao, F.; Alfieri, L.; Hirabayashi, Y.; Bianchi, A.; Mongelli, I.; Frieler, K.; Betts, R.A.; Feyen, L. Increased human and economic losses from river flooding with anthropogenic warming. Nat. Clim. Chang. 2018, 8, 781–786. https://doi.org/10.1038/s41558-018-0257-z.
6. Kundzewicz, Z.W.; Kanae, S.; Seneviratne, S.I.; Handmer, J.; Nicholls, N.; Peduzzi, P.; Mechler, R.; Bouwer, L.M.; Arnell, N.; Mach, K.; Muir-Wood, R.; Brakenridge, G.R.; Kron, W.; Benito, G.; Honda, Y.; Takahashi, K.; Sherstyukov, B. Flood risk and climate change: global and regional perspectives. Hydrol. Sci. J. 2014, 59, 1–28. https://doi.org/10.1080/02626667.2013.857411.
7. Hirabayashi, Y.; Mahendran, R.; Koirala, S.; Konoshima, L.; Yamazaki, D.; Watanabe, S.; Kim, H.; Kanae, S. Global flood risk under climate change. Nat. Clim. Chang. 2013, 3, 816–821. https://doi.org/10.1038/nclimate1911.
8. Arnell, N.W.; Gosling, S.N. The impacts of climate change on river flood risk at the global scale. Clim. Change 2016, 134, 387–401.
9. Mondal, A.; Lakshmi, V.; Hashemi, H. Intercomparison of trend analysis of multi satellite monthly precipitation products and gage measurements for river basins of India. J. Hydrol. 2018, 565, 779–790. https://doi.org/10.1016/j.jhydrol.2018.08.010.
10. Lakshmi, V. Remote sensing of the terrestrial water cycle; John Wiley & Sons: Hoboken, NJ, USA, 2019.
11. Dandridge, C.; Lakshmi, V.; Bolten, J.; Srinivasan, R. Evaluation of satellite-based rainfall estimates in the Lower Mekong River Basin. Remote Sens. 2019, 11, 2709. https://doi.org/10.3390/rs11222709.
12. Maidment, R.I.; Grimes, D.I.F.; Allan, R.P.; Greatrex, H.; Rojas, O.; Leo, O. Evaluation of satellite based and model re analysis rainfall estimates for Uganda. Meteorol. Appl. 2013, 20, 308-317.
13. Kidd, C.; Levizzani, V. Status of satellite precipitation retrievals. Hydrol. Earth Syst. Sci. 2011, 15, 1109–1116.
14. Huffman, G.J.; Bolvin, D.T.; Braithwaite, D.; Hsu, K.; Joyce, R.; Xie, P. Integrated Multi satellite Retrievals for GPM (IMERG) algorithm theoretical basis document; NASA Goddard Space Flight Center, 2020. Available online: https://gpm.nasa.gov (accessed on 15 April 2024).
15. Funk, C.; Peterson, P.; Landsfeld, M.; Pedreros, D.; Verdin, J.; Rowland, J.; Michaelsen, J. The climate hazards infrared precipitation with stations—a new environmental record for monitoring extremes. Sci. Data 2015, 2, 150066. https://doi.org/10.1038/sdata.2015.66.
16. Beck, H.E.; Vergopolan, N.; Pan, M.; Levizzani, V.; van Dijk, A.I.J.M.; Weedon, G.P.; Brocca, L.; Pappenberger, F.; Huffman, G.J.; Wood, E.F. Global-scale evaluation of 22 precipitation datasets using gauge observations and hydrological modeling. Hydrol. Earth Syst. Sci. 2017, 21, 6201–6217. doi:10.5194/hess-21-6201-2017.

 doi:10.20944/preprints202505.1570.v1




17. Maidment, R.I.; Grimes, D.; Black, E.; Tarnavsky, E.; Young, M.; Greatrex, H.; Allan, R.P.; Stein, T.H.M.; Nkonde, E.; Senkunda, S.; et al. A new, long-term daily satellite-based rainfall dataset for operational monitoring in Africa. Sci. Data 2017, 4, 170063. doi:10.1038/sdata.2017.63.
18. Le, M.-H.; Lakshmi, V.; Bolten, J.; Bui, D. Adequacy of satellite derived precipitation estimate for hydrological modeling in Vietnam basins. J. Hydrol. 2020, 586, 124820. https://doi.org/10.1016/j.jhydrol.2020.124820.
19. Tran, D.; Le, M.-H.; Zhang, R.; Nguyen, B.; Bolten, J.; Lakshmi, V. Robustness of gridded precipitation products for Vietnam basins using the comprehensive assessment framework of rainfall. Atmos. Res. 2023, 293, 106293.
20. Prat, O.P.; Nelson, B.R. Evaluation of precipitation estimates over CONUS derived from satellite, radar, and rain gauge data sets at daily to annual scales (2002–2012). Hydrol. Earth Syst. Sci. 2015, 19, 2037–2056. doi:10.5194/hess-19-2037-2015.
21. Hashemi, H.; Nordin, M.; Lakshmi, V.; Huffman, G.; Knight, R. Bias correction of long term satellite monthly precipitation product (TRMM 3B43) over the conterminous United States. J. Hydrometeorol. 2017, 18, 2491–2509. https://doi.org/10.1175/JHM-D-17-0025.1.
22. Zhang, S.; Wang, D.; Qin, Z.; et al. Assessment of the GPM and TRMM precipitation products using the rain gauge network over the Tibetan Plateau. J. Meteorol. Res. 2018, 32, 324–336. doi:10.1007/s13351-018-7067-0.
23. Dandridge, C.; Lakshmi, V.; Bolten, J.; Srinivasan, R. Evaluation of satellite based rainfall estimates in the Lower Mekong River Basin. Remote Sens. 2019, 11, 2709. https://doi.org/10.3390/rs11222709.
24. Alijanian, M.; Rakhshandehroo, G.R.; Mishra, A.K.; Dehghani, M. Evaluation of satellite rainfall climatology using CMORPH, PERSIANN-CDR, PERSIANN, TRMM, MSWEP over Iran. Int. J. Climatol. 2017, 37, 4896–4914. doi:10.1002/joc.5131.
25. Ayehu, G.T.; Tadesse, T.; Gessesse, B.; Dinku, T. Validation of new satellite rainfall products over the Upper Blue Nile Basin, Ethiopia. Atmos. Meas. Tech. 2018, 11, 1921–1936. doi:10.5194/amt-11-1921-2018.
26. Fayne, J.; Hashemi, H.; Huffman, G.; Lakshmi, V. Very high resolution altitude corrected, TMPA based monthly satellite precipitation product over the CONUS. Sci. Data 2020, 7, 96. https://doi.org/10.1038/s41597-020-0411-0.
27. Tran, D.; Nguyen, B.; Zhang, R.; Aryal, A.; Grodzka Lukaszewska, M.; Sinicyn, G.; Lakshmi, V. Quantification of gridded precipitation products on the Mekong River Basin: A case study for the Srepok River subbasin, Central Highland Vietnam. Remote Sens. 2023, 15, 1030. https://doi.org/10.3390/rs15041030.
28. Nash, J.E.; Sutcliffe, J.V. River flow forecasting through conceptual models part I—A discussion of principles. J. Hydrol. 1970, 10, 282–294. https://doi.org/10.1016/0022-1694(70)90255-6.
29. Gupta, H.V.; Sorooshian, S.; Yapo, P.O. Status of automatic calibration for hydrologic models: Comparison with multilevel expert calibration. J. Hydrol. Eng. 1999, 4, 135–143. https://doi.org/10.1061/(ASCE)1084-0699(1999)4:2(135).
30. Hashemi, H., M. Nordin, V. Lakshmi, G. J. Huffman, and R. Knight, 2017. Bias correction of long-term satellite monthly precipitation product (TRMM 3B43) over the conterminous United States. J. Hydrometeor., 18(9), 2491-2509. https://doi.org/10.1175/JHM-D-17-0025.1.
31. Massey, F.J. The Kolmogorov–Smirnov test for goodness of fit. J. Am. Stat. Assoc. 1958, 46, 68–76. https://doi.org/10.1080/01621459.1951.10500769.
32. Beguería, S.; Uncertainties in partial duration series modelling of extremes related to the choice of the threshold value. J. Hydrol. 2005, 303, 215–230. doi:10.1016/j.jhydrol.2004.07.015.
33. Koutsoyiannis D. Statistics of extremes and estimation of extreme rainfall: I. Theoretical investigation. Hydrol. Sci. J. 2004, 49, 575–590. doi:10.1623/hysj.49.4.575.54430.
34. Yu, Y.; Choi, Y.J.; Kim, J.H.; Lee, S. Evaluating the performance of satellite precipitation products for extreme rainfall detection. Remote Sens. 2022, 14, 567. https://doi.org/10.3390/rs14030567.
35. Doswell, C.A. III; Davies-Jones, R.; Keller, D.L. On summary measures of skill in rare event forecasting based on contingency tables. Wea. Forecasting 1990, 5, 576–585. doi:10.1175/1520-0434(1990)005<0576:OSMOSI>2.0.CO;2.

 doi:10.20944/preprints202505.1570.v1




36. Jolliffe, I.T.; Stephenson, D.B. Forecast Verification: A Practitioner's Guide in Atmospheric Science, 2nd ed.; John Wiley & Sons: Hoboken, NJ, USA, 2012.
37. Schaefer, J.T. The critical success index as an indicator of warning skill. Wea. Forecasting 1990, 5, 570–575. doi:10.1175/1520-0434(1990)005<0570:TCSIAA>2.0.CO;2.
38. Marzban, C. Scalar measures of performance in rare-event situations. Wea. Forecasting 1998, 13, 753–763. doi:10.1175/1520-0434(1998)013<0753:SMOPIR>2.0.CO;2.
39. Wilks, D.S. Statistical Methods in the Atmospheric Sciences, 3rd ed.; Academic Press: Amsterdam, The Netherlands, 2011.
40. Le, M.-H.; Lakshmi, V.; Bolten, J.; Bui, D. Adequacy of satellite-derived precipitation estimate for hydrological modeling in Vietnam basins. J. Hydrol. 2020, 586, 124820. doi:10.1016/j.jhydrol.2020.124820.
41. United States Geological Survey. Shuttle Radar Topography Mission (SRTM) elevation data; USGS: Reston, VA, USA, 2000. Available online: https://www.usgs.gov (accessed on 18 April 2024).
42. Gupta, P.; Singh, P.; Singh, P.; Joshi, V. Assessment of satellite based precipitation products for hydrological applications in the Himalayan region. J. Hydrol. 2020, 591, 125579. https://doi.org/10.1016/j.jhydrol.2020.125579.
43. Hordofa, T.; Kiggundu, N.; Girma, M. Performance evaluation of satellite based rainfall estimates for drought monitoring in the Upper Blue Nile Basin, Ethiopia. Meteorol. Appl. 2021, 28, e2007. https://doi.org/10.1002/met.2007.
44. Pearson, K. Notes on regression and inheritance in the case of two parents. Proc. R. Soc. Lond. 1895, 58, 240–242. https://doi.org/10.1098/rspl.1895.0041.
45. Chai, T.; Draxler, R.R. Root mean square error (RMSE) or mean absolute error (MAE)?—Arguments against avoiding RMSE in the literature. Geosci. Model Dev. 2014, 7, 1247–1250. https://doi.org/10.5194/gmd-7-1247-2014.
46. Willmott, C.J.; Matsuura, K. Advantages of the mean absolute error (MAE) over the root mean square error (RMSE) in assessing average model performance. Clim. Res. 2005, 30, 79–82. https://doi.org/10.3354/cr030079.
47. Tang, G.; Clark, M.P.; Papalexiou, S.M.; Ma, Z.; Hong, Y. Have satellite precipitation products improved over the last two decades? A comprehensive comparison of GPM IMERG with nine satellite and reanalysis datasets. Remote Sens. Environ. 2020, 240, 111697. https://doi.org/10.1016/j.rse.2020.111697.
48. Zhang, X.; Zhang, L.; Zhao, J.; Duan, J.; Liu, X. Assessment of the accuracy of satellite based precipitation products in the Tibetan Plateau. Water 2020, 12, 510. https://doi.org/10.3390/w12020510.
49. Peng, J.; Loew, A.; Chen, X.; Ma, Y.; Su, Z. Assessing the quality of satellite based precipitation estimates over the Tibetan Plateau. Atmos. Res. 2021, 249, 105307. https://doi.org/10.1016/j.atmosres.2020.105307.
50. Spearman, C. The proof and measurement of association between two things. Am. J. Psychol. 1904, 15, 72–101. https://doi.org/10.2307/1412159.
51. Draper, N.R.; Smith, H. Applied regression analysis, 3rd ed.; John Wiley & Sons: New York, NY, USA, 1998.
52. Da Silva, N.A.; Webber, B.G.M.; Matthews, A.J.; Feist, M.M.; Stein, T.H.M.; Holloway, C.E.; Abdullah, M.F.A.B. Validation of GPM IMERG extreme precipitation in the Maritime Continent by station and radar data. Earth Space Sci. 2021, 8, e2021EA001738. https://doi.org/10.1029/2021EA001738.
53. Ji, H.; Peng, D.; Gu, Y.; Liang, Y.; Luo, X. Evaluation of multiple satellite precipitation products and their potential utilities in the Yarlung Zangbo River Basin. Sci. Rep. 2022, 12, 14071. https://doi.org/10.1038/s41598-022-17551-y.
54. Hameed, I.A.; Al Nuaimi, K.; Idrees, N.M. Reliability of GPM IMERG satellite precipitation data for modelling flash flood events in selected watersheds in the UAE. Remote Sens. 2023, 15, 3991. doi:10.3390/rs15163991.
55. Thom, H.C.S. A note on the gamma distribution. Mon. Weather Rev. 1958, 86, 117–122. https://doi.org/10.1175/1520-0493(1958)086<0117:ANOTGD>2.0.CO;2.
56. Aitchison, J.; Brown, J.A.C. The lognormal distribution; Cambridge University Press: Cambridge, UK, 1957.
57. Fisher, R.A. On the mathematical foundations of theoretical statistics. Philos. Trans. R. Soc. Lond. A 1922, 222, 309–368. https://doi.org/10.1098/rsta.1922.0009.
58. Weibull, W. A statistical distribution function of wide applicability. J. Appl. Mech. 1951, 18, 293–297.

 doi:10.20944/preprints202505.1570.v1




59. Johnson, N.L.; Kotz, S.; Balakrishnan, N. Continuous univariate distributions; Wiley: New York, NY, USA, 1994; Volume 1, 2nd ed.
60. Gumbel, E.J. Statistics of extremes; Columbia University Press: New York, NY, USA, 1958.
61. Pareto, V. Cours d'économie politique; Rouge: Lausanne, Switzerland, 1896.
62. Jenkinson, A.F. The frequency distribution of the annual maximum (or minimum) values of meteorological elements. Q. J. R. Meteorol. Soc. 1955, 81, 158–171. https://doi.org/10.1002/qj.49708134804.
63. Ebert, E.E.; Damrath, U.; Wergen, W.; Baldwin, M.E. The WGNE assessment of short-term quantitative precipitation forecasts. Bull. Am. Meteorol. Soc. 2007, 84, 483–494. https://doi.org/10.1175/BAMS-84-4-483.
64. Öztopal, A. Forecast verification: A practitioner's guide in atmospheric science. Meteorol. Atmos. Phys. 2007, 101, 279–280.
65. Aksu, H.; Akgül, M.A. Performance evaluation of CHIRPS satellite precipitation estimates over Turkey. Theor. Appl. Climatol. 2020, 142, 71–84. https://doi.org/10.1007/s00704-020-03277-0.
66. Hisam, E. Evaluation of grid based precipitation products over the Mediterranean region in Turkey. M.S. Thesis, İstanbul Technical University, Graduate School, İstanbul, Turkey, 2022. Available online: http://hdl.handle.net/11527/25494 (accessed on 18 October 2024).
67. Hafizi, H.; Sorman, A.A. Performance assessment of CHIRPSv2.0 and MERRA 2 gridded precipitation datasets over complex topography of Turkey. Environ. Sci. Proc. 2022, 19, 21. https://doi.org/10.3390/ecas2022-12815.
68. Aksu, H.; Taflan, G.Y.; Yaldiz, S.G.; Akgül, M.A. Evaluation of IMERG for GPM satellite-based precipitation products for extreme precipitation indices over Turkiye. Atmos. Res. 2023, (article 106826). https://doi.org/10.1016/j.atmosres.2023.106826.
69. Aksu, H.; Yaldiz, S.G.; Taflan, G.Y.; Akgül, M.A. Frequency analysis based on peaks-over-threshold approach for GPM IMERG precipitation product. Theor. Appl. Climatol. 2023, 154, 275–289. https://doi.org/10.1007/s00704-023-04056-9.
70. Koçak, R.; Dönmez, S.; Tor, M.A.; Tekeli, A. Utilizing GPM IMERG early, late and final runs for flood estimation over Aralık district, Iğdır City. In Proceedings of the XXVIII General Assembly of the International Union of Geodesy and Geophysics (IUGG), Berlin, Germany, 2023. https://doi.org/10.57757/IUGG23-0462.
71. Koçak, R.; Tor, M.A.; Dönmez, S.; Tekeli, A.E. Iğdır İli Aralık İlçesi sellerinin GPM uydu yağış verilerinden ilk ve son ürünleri ile incelenmesi. In Proceedings of the VIII Remote Sensing GIS Symposium (UZAL CBS 2022), Ankara, Turkey, 2022. https://doi.org/10.15659/uzalcbs2022.12801.